Understanding printed hexagonal contacts for large area solar cells through simulation and experiment

*Selen Solak, Sara Shishegaran, Arved Hübler**

Institute for Print and Media Technology, Chemnitz University of Technology, Printed Electronics
E-mail:arved.huebler@mb.tu-chemnitz.de

*Roderick C. I. MacKenzie**
Faculty of Engineering, The University of Nottingham, University Park, Nottingham, NG7 2RD
E-mail: roderick.mackenzie@nottingham.ac.uk

Keywords: Solar-energy; modelling; large-area; printed solar cells

Abstract

Since their conception, organic electronic semiconductors have promised large area optoelectronic devices that can be mass produced at a fraction of the cost and embodied energy of devices made from traditional semiconductors. However, up-scaling from small area lab-scale fabrication techniques to large area roll-to-roll production has proved a substantial challenge. At the heart of this up-scaling problem is the need for low cost, reliable contacts which can be readily printed. Device performance is often limited by the contacts, in terms of charge extraction efficiency and morphological compatibility of the sequentially deposited layers. Herein, we combine high-speed roll-to-roll flexographic and gravure printing with numerical device modeling to understand the performance of printed silver hexagonal contacts, and how contact design can affect final device performance. We present a strategy, which we dub ’virtual up scaling’ where by the performance of the printed contact is virtually evaluated with an active layer material/device structure before the full device stack is printed. Through this methodology we develop a set of general design rules which can be applied when experimentally optimizing contacts of optoelectronic devices. This approach has the potential to significantly reduce the number of design iterations and thus print runs when up-scaling a structure.

1. Introduction

In recent years, novel thin film materials have been used in a wide range of devices including bio-sensors,[1,2] photovoltaics[3] and displays.[4, 5] These material systems offer the panacea of a low cost, flexible device with a low energy input and the associated reduction in CO_2 emission during fabrication.[6] For this to be achieved, however, the highly promising small area lab scale devices have to make their way from the spin coater to high speed large area mass production.[7] Among the many material systems people have tried to print (including Perovskites[8] and PbS quantum dots[9]) organic materials lend themselves especially well to traditional printing techniques. Printing processes are also ideal for applying solar cells to light and flexible substrates and printing very large areas in a non-stop mass production environment. This is because they are soluble meaning they can be easily formulated into inks, that must adhere to the various substrates. Established printing methods such as flexographic, gravure and screen printing, make possible sheet-to-sheet and high throughput roll-to-roll production.[8]

Until recently, however these printing technologies were most often only applied to small area lab scale devices (~ 1cm^2) and mostly under clean room conditions. To avoid issues of surface energy/surface tension mismatches. More problematic layers such as the contacts, and buffer layers were still deposited using spin coating or vacuum evaporation.[10,11] For thin film devices to reach their true potential, full sequentially roll-to-roll production of all layers must be achieved.

There has already been much work on printing large homogeneous layers and maintaining device performance during up-scaling.[12] The larger the printed film, the more probable it is to contain defects, such as a pinhole or a short. In solar cells this limitation has in general confined their design to narrow strips.[13] In roll-to-roll device fabrication, the key challenge is to subsequently deposit all layers of the device in continuous production.[14]

Printing high quality films on top of each other is a fundamentally difficult problem because; 1) each material will have a different viscosity making the way it interacts with the printing process, substrate and under layer different from layer to layer; 2) each layer/ink will have a different surface energy/surface tension, meaning some inks may simply bubble and face problems with adhesion; 3) optimum drying rates which are dictated by print speed and the drying unit are very different from material to material; and 4) The final layer quality, electrical and optical properties are affected by a combination of the chosen printing method, the materials, the specific printing parameters and post processing conditions.

For the above reasons, taking a successful small area device and optimizing it for printing is an arduous process and often requires the device structure/materials to be significantly changed. Even if one manages to achieve well printed layers on a large scale, the final device may not be optimum for the desired application (i.e. solar modules light harvesting or bio-sensing). Furthermore, it is difficult to tell how the device will perform before the printing protocols have been developed for each layer and the entire stack built. Once the device has been finally printed and tested, the performance of the device will have to be further optimized, through an iterative process, of adjusting device geometry/morphology through adjustments to the printing process. Very often a device which is electronically optimized may be impossible to print, while a device optimized for the printing process may perform badly. Added to these difficulties, printed devices tend to be larger requiring more material and making them more expensive, this is why the community generally (especially in smaller labs) avoids printing devices and progress in this area has been slow.

Herein, we focus on design of hexagonal contacts for solar cells however, the methods developed can equally be applied to other classes of opto-electronic devices. We demonstrate that by combining printing and simulation, one can get a good understanding of how a given contact will perform in a final device before the finished device is fabricated. We demonstrate that by using this method the print design can be optimized for a given device architecture of solar cell before the entire device stack is printed, we dub this method 'virtual up scaling'. This method has the potential to reduce the number of print runs/investment needed to transfer a device from the lab to high volume production. Using this approach we are able to estimate the optical/electrical losses which occur in the contact/buffer layers, and ultimately estimate power conversion efficiency for a large area device from a small area device before printing commences. The paper culminates in a set of design rules for silver hexagonal contacts.

2. Experiment

Within this section we print example PEDOT:PSS/hexagonal Ag contacts using a combination of gravure and flexographic printing. It should be noted that the print runs presented in this section took over 6 months to perform and this length of development cycle is typical for broad area printed devices. It is these long development cycles which prevent efficient iterative/rapid improvement of broad area devices. The latter half of the paper uses input parameters obtained from these experiments to accelerate device optimization through simulation as a potential way of short cutting the development cycle.

Although previously many different semi-transparent contact structures have been proposed, [19] within this work we focus on hexagonal silver contacts because they have been used widely in organic electronics due to their ability to geometrically pack efficiently. The substrate used for the fabrication process was a 125 μ*m* thick polyethylene terephthalate (PET) roll (Melinex 506) purchased from DuPont Teijin Films. Prior to printing the roll was corona treated at a speed of 0.2 ms^{-1} and at a power of 0.3 kW using an Arcotec Coronagenerator CG 06-2. The hexagonal contacts themselves were fabricated by a roll-to-roll (R2R) flexographic printing process which deposited a water based ink (PFI-722 from Novacentrix) containing silver nanoparticles. Flexographic printing has the advantage of being a fast with low material usage and able to produce printed lines with fine edges. The elastomer flexo sleeve and anilox roll were laser engraved by SWG GmbH. The R2R printing machine a LaborMan II, a laboratory printing machine called Laborman specially developed by MAN Roland AG, Augsburg, had a maximum web width of 140 mm and a 2 m long hot air dryer, which enables drying at 120 C. Next, a highly conductive PEDOT:PSS (poly(3,4-ethylenedioxythiophene) polystyrene sulfonate) ink CLEVIOS PH1000 (Heraeus GmbH) was R2R gravure printed on top of the silver layer, finally a ZnO (Zincoxide) Avantama N-12, 5 wt % in ethanol layer was gravure printed. Further details about the fabrication process can be found in the SI. All layers are dried at $120^{O}C$ for 3 min.

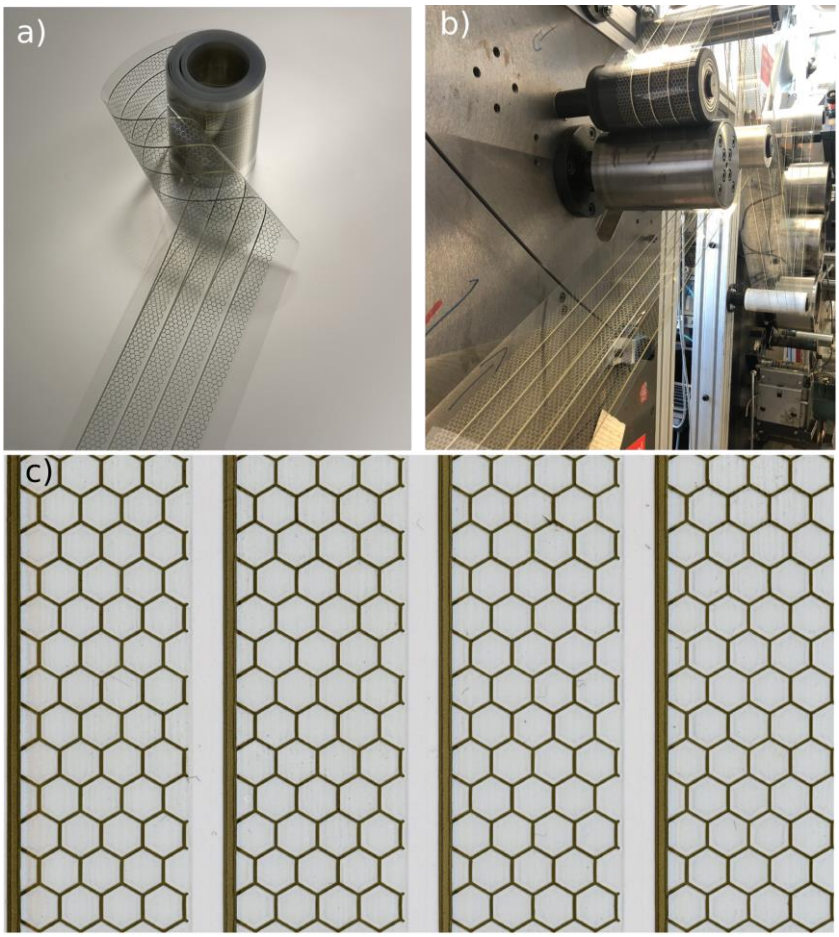

Figure 1. Printing the contact structures. a) The roll-to-roll printing unit used to fabricate the contacts. On average the lengths of the substrates were 1000 m long, this length of print run was needed to stabalize the printing process. b) The final roll-to-roll printed Ag hexagonal contacts/PEDOT:PSS/ZnO. c) An enlarged image of the final printed contact structures. Each printed finger in figure 1c measures 1.7cm wide and approximately 5cm tall, a detailed drawing of the structure can be found in the SI.

The roll-to-roll printing machine is visible in figure 1a, and an example of a finished 1000 meters long roll printed contact can be seen in figure 1b (the print run has to be long for the printing process to stabilize) and photographs of the final structures are shown in 2c.

The effect of printing parameters on the electrical and physical properties were studied for two different silver grids one with a pitch (distance between centers of the hexagons) of 2 mm and one with a pitch 5 mm. Both the 2 and 5 mm pitches were printed at speeds of 0.2, 0.4 and 0.75ms^{-1} . The 5 mm pitch was printed with three different anilox volumes, 1.5 ml m^{-2}, 4 ml m^{-2}, 10 ml m^{-2}, while the 2 mm pitch was printed with one anilox volume of 4 .

Microscope images, showing how these printing speeds influenced film quality can be seen in table 2. It can be seen that line width is not a strong function of the print speed. However the line thickness does increase as a function of increasing anilox volume (also see SI). Narrower lines mean a higher resistance, it also means the contacts are more prone to cracking. Printing with a pitch of 5 *mm*, anilox volume of of 10 ml m^{-2} at 0.75 ms^{-1} produces the smoothest layer. A low roughness value is important as any material protruding into the subsequently deposited layers can form a short circuit. The thickness and roughness values for each sample can be found in the SI.

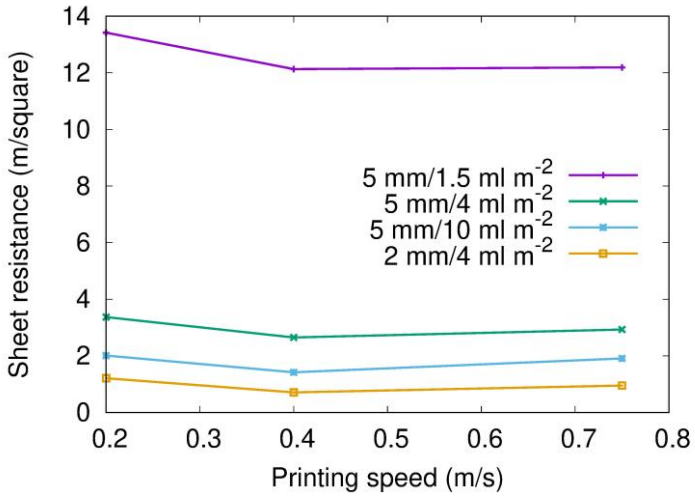

Figure 2. Sheet resistance (R_s) of the silver contact structures versus printing speed for samples with a range of and printing pitches (mm) and anilox transfer volumes (ml m^{-2}), these values were measured using a four point probe directly on the thick Ag strip to the left of figure 1c

The sheet resistance (R_s) as measured with a four point probe for different different speeds are shown in figure 2. It can be seen that the 5 mm /1.5ml m^{-2} printed contacts have the highest sheet resistance. By examining the microscope images in table 2 it can be seen that this corresponds to the samples with the thinnest line width. The 2 mm/ 4 ml m^{-2} samples in general have the lowest resistance again by comparing with table 2 it can be seen to correspond to the thickest line widths. As would be expected by inspection of the microscope images, changes in the print speed don't change the conductivity significantly.

After flexographic printing of the silver grids, PEDOT:PSS was R2R gravure printed on top, printing speed was kept same for all the layers at 2 ms^{-1}. Thickness and sheet resistance (R_s) values of the silver grid alone, Ag/PEDOT:PSS and Ag grid/PEDOT:PSS/ZnO are shown in table 1, along with the transmittance of the material.

Table 1. Thickness and sheet resistance (R_s) of 5mm pitch Ag grid, Ag/PEDOT:PSS and Ag/PEDOT:PSS/ZnO. For the top line of the table (Ag) R_s was measured using a four point probe placed directly on the wide metallic strip on the left of figure 1c. For the middle line of the table (Ag/PEDOT:PSS) the resistance value was taken again using a four point probe but this time placed in the center of the printed cells. (a) thickness is the sum of PEDOT:PSS and ZnO. For values of resistance averaged over multiple printed cells see the SI.

Structure	T @ 550 nm (%)	Thickness (nm)	Roughness (nm)	R_s (Ω/sq)
Ag	75.2	683.15	-	0.85
Ag/PEDOT:PSS	72.2	54.69	5.25	1.37
Ag/PEDOT:PSS/ZnO	67.8	114.94[a]	5.51	-

From the above it is clear that the printed line width can significantly affect the conductivity of the contacts. Also looking at the microscope images it is clear that the contacts printed with a 5 *mm* pitch will not block much light, while those with a 2 *mm* will block a significant amount of light. Furthermore, although we did not conduct mechanical fatigue experiments, if one examines the microscope images, the thin lines printed with slow speeds and low volumes look fragile, and one would expect these contacts to fare less well when subject to mechanical stresses. Conversely, the samples with thicker lines will block more light and are more conductive.

At this point it is not clear which contact structure would be optimum for a solar cell and how we can trade thickness/conductivity off against ability to harvest light. It is clear that low anilox volumes at low speed probably produce fragile contacts and thicker line widths will have better conductivities. The next step would be to to make an educated guess as to which would be the optimum contact and proceed with deposition of a device. However, it should be highlighted that from the practical perspective an exhaustive experimental search of the parameter space for an optimum structure is a difficult proposition. These long development

times and the inability to efficiently search the parameter space are the key challenge in up-scaling organic electronic devices through printing.

Table 2: a) Microscopy images (2.5x magnification) for different printing speeds 0.2 ms^{-1}, 0.4 ms^{-1} , 0.75 ms^{-1} and different anilox volumes 1.5 ml m^{-2}, 4 ml m^{-2} , 10 ml m^{-2} for 5 mm pitch and 4 ml m^{-2} for 2 mm pitch.

	Printing speed		
Sample pitch Anilox volume	0.2 ms^{-1}	0.4 ms^{-1}	0.75 ms^{-1}
5 mm/ 1.5 ml m^{-2}	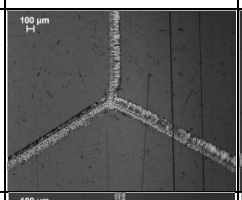	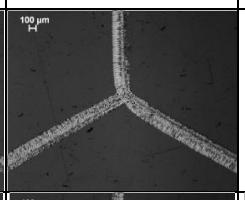	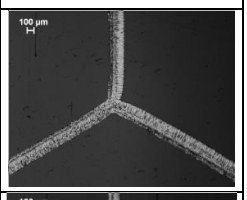
5 mm/ 4 ml m^{-2}	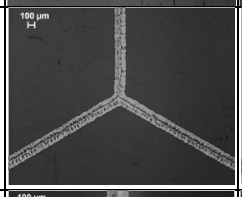	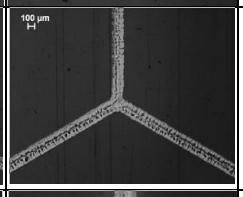	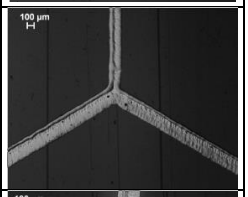
5 mm/ 10 ml m^{-2}	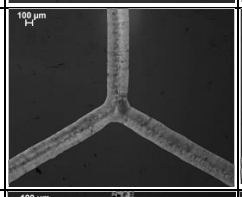	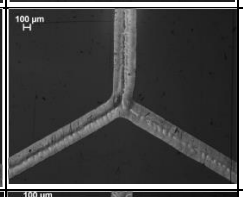	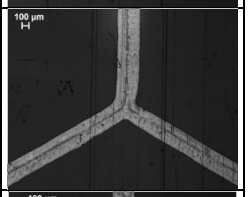
2 mm/ 4 ml m^{-2}	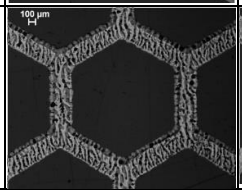	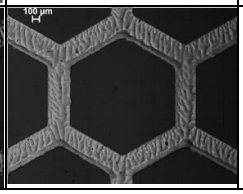	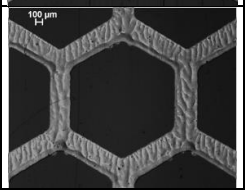

3. Simulation

Using the experimental results from the previous section as a starting point, in this section we use modeling to understand how far our contacts are from the optimum, and what an optimum contact structure would look like. We then take a small area organic PM6:Y6 solar cell from the literature and use it's structure along with it's electrical performance to estimate how it would perform were it upscaled on top of our printed contacts, we dub this method 'virtual up-scaling'. The simulation is constrained by the experimental results from the previous section in that the resistivities of the Ag were set at $4.3x10^{-7}$ Ωm, and the values used for PEDOT:PSS were $1x10^{-5}$ Ωm which represent typical values of the printed layers. Line

widths were constrained to experimentally reasonable values of between 0.1 - 1.5 mm, which would be readily fabricatable using our printing process.

The virtual up-scaling of a contact structure has five steps; 1) Draw out the contact structures one wishes to simulate in a 2D map form (see figure 3a); 2) discretize the image using a triangular mesh to capture it's shape in 3D and then simplify the mesh using a vertex removal approach[15] (see figure 3 a,b); 3) Use this shape and measured values of resistance to build a 3D circuit diagram representing the device (see figure 3c). In figure 3c silver is represented by red resistors and the PEDOT:PSS by green resistors; 4) build this contact structure into a virtual solar cell by adding representative diodes; and 5) use this structure to understand the electrical and optical properties of the contacts/device. The general purpose photovoltaic device model (gpvdm) was adapted to perform these steps, see SI for further information.[17,18]

By applying a voltage and measuring the current between where current would be generated by the active layer and where current would leave the device, we are able to map out the resistance of the contact structure as a function of position. Figure 3d, shows the spatial resistance of a single finger of a hexagonal contacts. It can be seen from figure 3d, that the resistance directly under the Ag grid is very low, and the overall resistance increases as one moves away from the left hand contact.

The light absorbed within the 3D structure is calculated using the transfer matrix method.[16] The fraction of the light which passes through metal grid is depicted in figure 4 (top) as a function of both printed cell width and line width. It can be seen that the fraction of light the grid absorbs only becomes significant (>20%) once the cell width drops below 3.5mm and line widths become large. Figure 4 (bottom) plots the resistance of the strip of honeycombs as measured from the far right 20% of the PEDOT:PSS in figure 3c to the far left Ag grid where current would leave the device. Measuring current in this way is equivalent to placing a copper conducting strip on right 20% of the PEDOT:PSS in figure 3c and using a multimeter to experimentally determine the resistance to the extracting contact. As the width of the honeycomb cell increases the resistance of the structure also increases, line width is not seen to have a significant effect. Any grid structure below 5mm could be seen as optimal from the perspective of electrical conductivity.

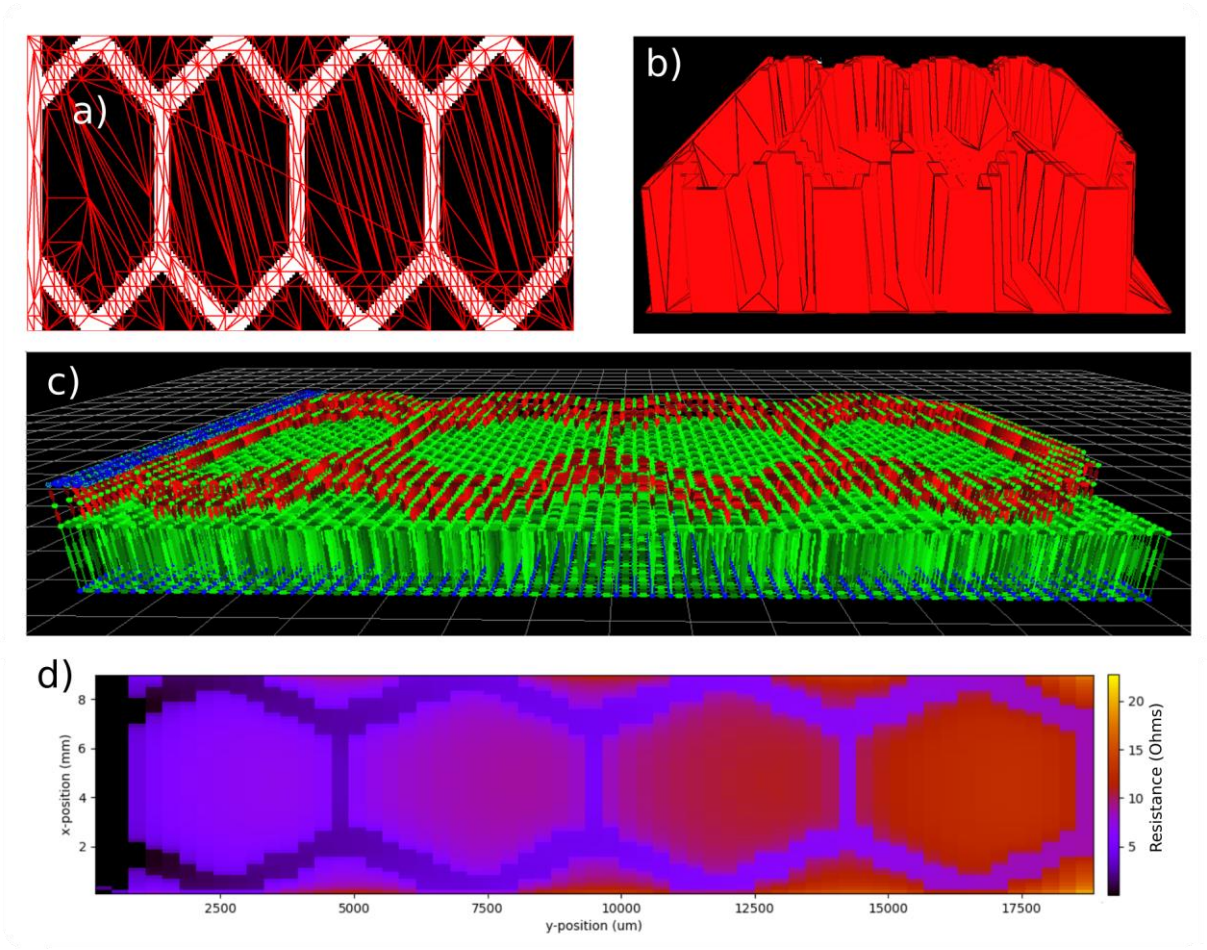

Figure 3. a) An example simulated contact structure drawn in 2D (white), with a triangular mesh superimposed over it (red); b) The triangular mesh of figure a expanded to 3D ready for electrical/optical simulation; c) A 3D circuit diagram of the contact, the green resistors represent the PEDOT:PSS, the red resistors represent the Ag; d) a calculated resistance plot of entire contact structure.

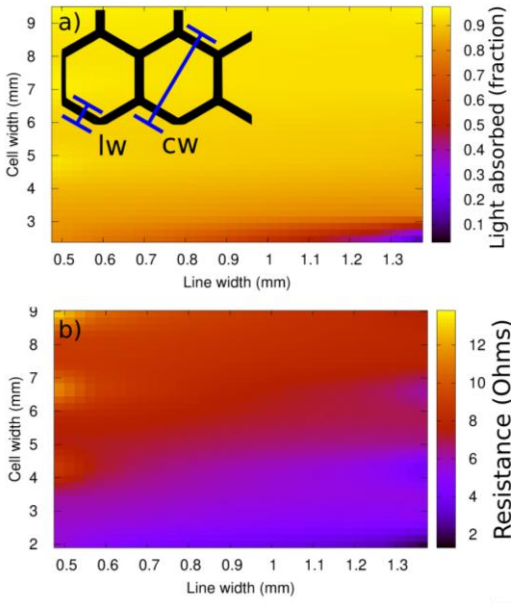

Figure 4. a) Light absorbed in the PEDOT:PSS layer; b) Resistance of the contact measured by the average resistance between the bottom of the PEDOT:PSS and the extracting contact on the left; inset) A diagram showing the line width and cell width.

To understand how the printed contacts would perform in a finished solar cell we take a small area state-of-the-art small molecule acceptor PM6:Y6 device from the literature[20]. We calculate the photocurrent for the 1D structure using the transfer matrix method and then use the Shockley diode equation to fit to the light current voltage curves of the cell. The result of these fits and band diagrams are presented in figure **5**.

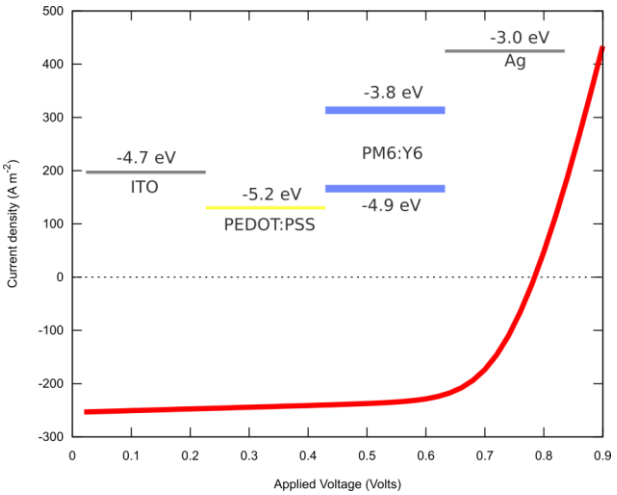

Figure 5. A fit of the Shockley diode equation equation to the JV curve representing a modern small molecule/acceptor device. The original experimental data on which the fit is based can be found in Yao et al[20] and has been reproduced under terms of the CC-BY license.

The hole transporting PEDOT:PSS layers were then virtually removed from the structures devices depicted in 5, and replaced with a simulated PEDOT:PSS/Ag honeycomb. The 1D device model was then expanded to 3D, see figure 6, new 3D absorption profiles were calculated using the transfer matrix method across the device. Using this circuit diagram, the JV curves for hexagonal structures with a range of diameters and print line widths were simulated.

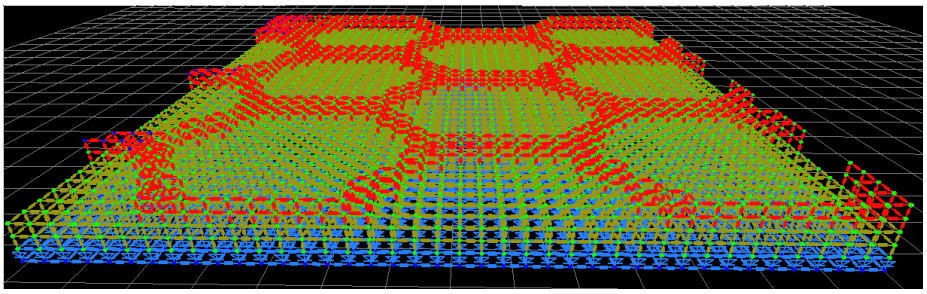

Figure 6. A schematic circuit diagram of a the simulated PM6:Y6 device, the diodes representing the active layer can be seen in blue, the resistors representing the PEDOT:PSS in green and the resistors representing the Ag contact in red.

Figure 7, plots the values of fill factor, PCE, V_{oc} and J_{sc} for a range of honeycomb cell widths and line widths. It can be seen that as the cell width is increased to over 6mm and line width decreased below 0.6mm the fill factor drops to below 0.5. This can be explained by the fact that for ever thinner and wider cells the more resistance will be placed between the photogeneration location of charge and the point at which it can be conducted along the honeycomb mesh. V_{oc} does not seem to be significantly affected by the contact structure it's self, although in a real device with an inhomogeneities introduced in the active layer during the printing process, one would expect a variation. If one compares the figure denoting J_{sc} to that of resistance in figure 4, it can be seen that the figures are almost the inverse of each other, printed contact structure designs with low resistance seem to produce values of J_{sc} at around -20 Am^{-2} while designs with high resistance seem to values of around -100 Am^{-2}. This trend can not be explained by drop in light absorption show in figure 4.

To explain the trend in J_{sc} we need to remember that the device is non linear and shading by the contacts will bias each section of the active layer at a different point on the JV curve. Those sections of material which are exposed to light will be contributing negative photocurrent to J_{sc}, however those sections of material directly under the contacts will not be able to contribute photocurrent, indeed these sections of material be exposed to a forward bias so will contributing a positive current to J_{sc}. They are in effect, actively short circuiting the active layer, this can be seen in Figure 8, where yellow represents positive current flow in the diodes under the metallic grid and the deeper colors represent photogenerated current. It is therefore clear that having a device with the minimum of shading possible is key to achieving high device efficiencies.

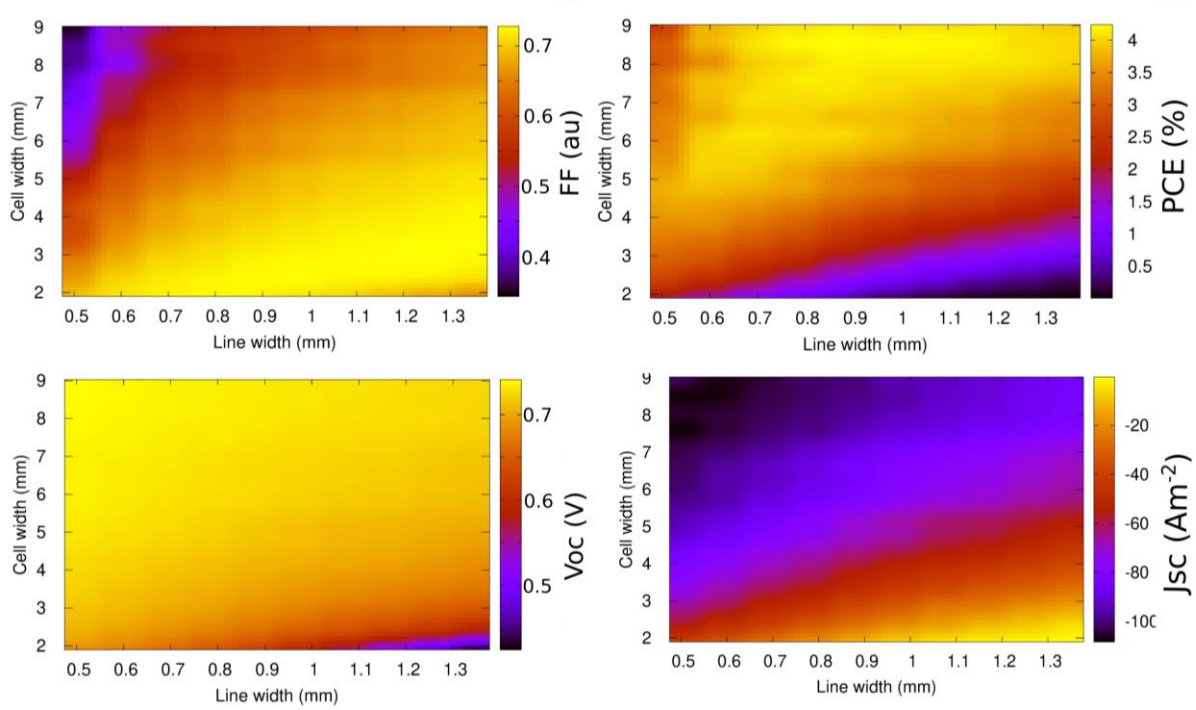

Figure 7. Clock wise, fill factor, PCE, V_{oc} and J_{sc} for the simulated PM6:Y6 structure as a function of hexagonal cell width line width.

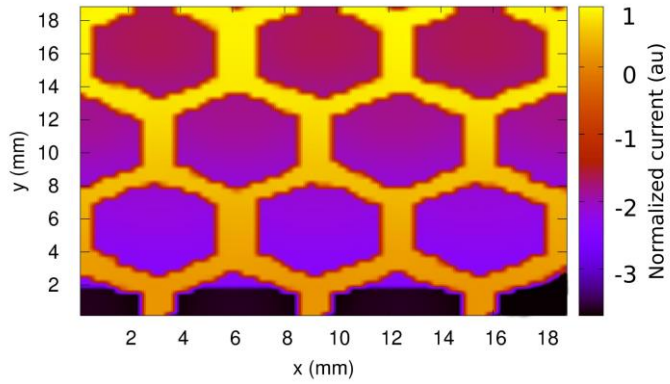

Figure 8. Normalized current flow through the diodes within the device, yellow represents positive current detracting from J_{sc}, and negative values represent diodes contributing photocurrent to J_{sc}.

Figure 9 plots the power conversion efficiency of the cell as a function of resistivity of both the PEDOT:PSS and the silver grid. From the plot it seems that increasing the conductivity of either the silver or the PEDOT:PSS has a positive influence on the power conversion

efficiency, it is not clear that one should prioritize one over the other when optimizing materials.

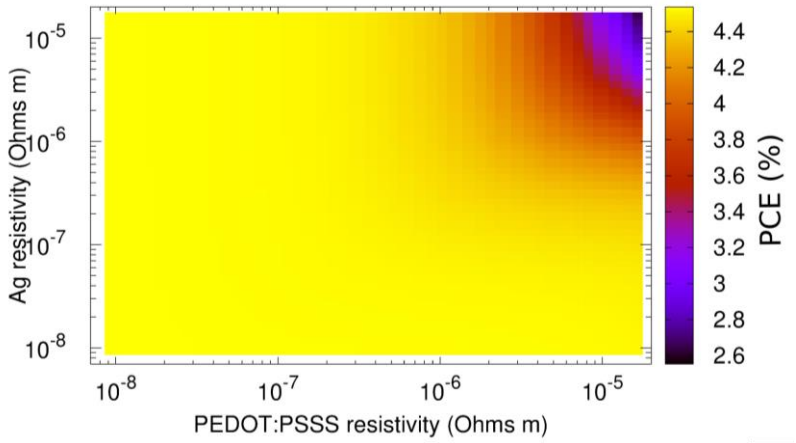

Figure 9. A plot of PCE as a function of PEDOT:PSS and Ag resistivity. It can be seen that increasing the resistivity of either the Ag grid or the PEDOT:PSS will be beneficial to device performance.

4. Conclusions

Above, we fabricated Ag contact structures using flexographic printing, after the contact structures were fabricated gravure printing was used to deposit layers of PEDOT:PSS and ZnO. We used these experiments to provide parameters as modeling inputs to understand how these contacts would behave in real world devices. We developed a method whereby an arbitrary contact structure could be drawn, and then the device simulated, and the performance estimated. Our simulations showed that shading by the contacts not only reduced light incident on the active layer, but also allowed the dark part of the active layer to act as a shunt resistor effectively shorting the layer. Furthermore, the PEDOT:PSS/Ag structure should be thought of as one layer, in that they can both conduct current laterally and thus an improvement in or the other should be seen as beneficial. Reducing resistivity in either layer will be beneficial to device performance. However, due to losses in J_{sc} caused by shading and the high conductivity of the Ag our recommendation would be to try to have line widths of the grid as thin as mechanically possible with the intention that diffuse light will be able to illuminate the material under the printed contact grid. Finally, we demonstrated that the use

of 'virtual up-scaling' can help choose design parameters before the entire stack is printed and brute-force optimized. This process can give a broad understanding losses in large area printed devices before they are fabricated.

Supporting Information

Supporting Information is available from the Wiley Online Library or from the author.

Acknowledgements

We thank Martin Mellendorf and Georg Schmidt for their support in the printing experiments and Mr. Thomas Weißbach for assistance with material issues.

Received: ((will be filled in by the editorial staff))
Revised: ((will be filled in by the editorial staff))
Published online: ((will be filled in by the editorial staff))

References

[1] C. Sun, X. Wang, M. A. Auwalu, S. Cheng, W. Hu, *EcoMat n/a*, n/a.

[2] N. Wang, A. Yang, Y. Fu, Y. Li, F. Yan, *Accounts of Chemical Research* **2019**, *52*, 2 277.

[3] S. Li, C.-Z. Li, M. Shi, H. Chen, *ACS Energy Letters* **2020**, *5*, 5 1554.

[4] X. Shi, Y. Zuo, P. Zhai, J. Shen, Y. Yang, Z. Gao, M. Liao, J. Wu, J. Wang, X. Xu, Q. Tong, B. Zhang, B. Wang, X. Sun, L. Zhang, Q. Pei, D. Jin, P. Chen, H. Peng, *Nature* **2021**, *591*, 7849 240.

[5] M. Choi, Y. J. Park, B. K. Sharma, S.-R. Bae, S. Y. Kim, J.-H. Ahn, *Science Advances* **2018**, *4*, 4.

[6] B. Azzopardi, C. J. M. Emmott, A. Urbina, F. C. Krebs, J. Mutale, J. Nelson, *Energy Environ. Sci.* **2011**, *4* 3741.

[7] A. Huebler, U. Hahn, W. Beier, N. Lasch, T. Fischer, In *2nd International IEEE Conference on Polymers and Adhesives in Microelectronics and Photonics. POLYTRONIC 2002. Conference Proceedings (Cat. No.02EX599)*. **2002** 172–176.

[8] Y. Y. Kim, T.-Y. Yang, R. Suhonen, A. Kemppainen, K. Hwang, N. J. Jeon, J. Seo, *Nature Communications* **2020**, *11*, 1 5146.

[9] M. Raissi, Y. Pellegrin, S. Jobic, M. Boujtita, F. Odobel, *Scientific Reports* **2016**, *6*, 1 24908.

[10] *Solar Energy Materials and Solar Cells* **2012**, *105* 77.

[11] M. M. Voigt, R. C. Mackenzie, C. P. Yau, P. Atienzar, J. Dane, P. E. Keivanidis, D. D. Bradley, J. Nelson, *Solar Energy Materials and Solar Cells* **2011**, *95*, 2 731.

[12] B. Fan, W. Zhong, L. Ying, D. Zhang, M. Li, Y. Lin, R. Xia, F. Liu, H.-L. Yip, N. Li, Y. Ma, C. J. Brabec, F. Huang, Y. Cao, *Nature Communications* **2019**, *10*, 1 4100.

[13] M. Finn, C. J. Martens, A. V. Zaretski, B. Roth, R. R. Søndergaard, F. C. Krebs, D. J. Lipomi, *Solar Energy Materials and Solar Cells* **2018**, *174* 7.

[14] A. Hübler, B. Trnovec, T. Zillger, M. Ali, N. Wetzold, M. Mingebach, A. Wagenpfahl, C. Deibel, V. Dyakonov, *Advanced Energy Materials* **2011**, *1*, 6 1018.

[15] W. J. Schroeder, J. A. Zarge, W. E. Lorensen, In *Proceedings of the 19th annual conference on Computer graphics and interactive techniques*. **1992** 65–70.

[16] P. Peumans, A. Yakimov, S. R. Forrest, *Journal of Applied Physics* **2003**, *93*, 7 3693.

[17] R. C. I. MacKenzie, C. G. Shuttle, M. L. Chabinyc, J. Nelson, *Advanced Energy Materials*, **2012**, 2, 662-669

[18] N. Majeed, M. Saladina, M. Krompiec, S. Greedy, C. Deibel, R. C. I. MacKenzie, *Advanced Functional Materials*, **2020**, 30, 1907259

[19] C. P.Muzzillo, Solar Energy Materials and Solar Cells, **2017**, 169, 68-77

[20] J. Yao, B. Qiu, Z.-G. Zhang, L. Xue, R. Wang, C. Zhang, S. Chen, Q. Zhou, C. Sun, C. Yang, M. Xiao, L. Meng, Y. Li, *Nature Communications* **2020**, *11*, 1 2726.

Supporting Information

Understanding printed hexagonal contacts for large area solar cells though simulation and experiment

Selen Solak, Sara Shishegaran, Arved Hübler and Roderick C. I. MacKenziooe

Further experimental detail

The silver ink PFI-722 with 60 % wt was purchased from Novacentrix. And the high conductive PEDOT:PSS (CLEVIOS™ PH1000) was purchased from Heraeus GmbH and the zinc oxide nanoparticle solution purchased from Avantama with 5 % wt. in ethanol (Avantama-N12). The gravure printer had two layouts with pitch sizes of 2 and 5 mm were printed which have 3 and 1 mm contact strip, respectively. The gravure cylinder has 15 ml m^{-2} transfer volume and layers are printed with 0.2 ms^{-1} printing speed. Microscopic imaging was done using an Axioskop 2 MAT mot from ZEIZZ. Thickness and roughness of printed the layers was measured by a Dektak XT Profilometer from BRUKER.

Detailed thickness and roughness tables

Due to the complex geometry of the structure, the four point probe could only be used on uniform regions such as directly on the thick line of Ag on the left hand side of the sample (see figure 1c) and in the center of the honeycomb. To measure the average resistance of multiple hexagonal structures a 17cm long section of the printed hexagonal grid was cut from taken the roll, the ends covered in conducting copper tape and a multimeter used to perform the measurement. This is reasonable because our device is so long that any contact resistance effects will be far smaller than bulk resistance effects.

Table S1. Sheet resistance of 2 mm and 5 mm pitch at different anilox volumes and printing speeds, measured with multimeter in large area (10 squares).

Sheet Resistance [Ω/sq]			
Sample	0.2 ms^{-1}	0.4 ms^{-1}	0.75 ms^{-1}
1.5 ml m^{-2} / 5 mm	13.42	12.13	12.19
4 ml m^{-2} / 5 mm	3.37	2.65	2.93
10 ml m^{-2} / 5 mm	2.01	1.42	1.91
4 ml m^{-2} / 2 mm	1.21	0.71	0.95

Table S2. Sheet resistance of 2 mm and 5 mm pitch at different anilox volumes and printing speeds, measured with four-probe method.

Thickness [nm]			
Sample	0.2 ms^{-1}	0.4 ms^{-1}	0.75 ms^{-1}
1.5 ml m^{-2} / 5 mm	156.63	103.72	154.56
4 ml m^{-2} / 5 mm	357.22	374.46	413.06
10 ml m^{-2} / 5 mm	337.06	339.02	343.05
4 ml m^{-2} / 2 mm	248.99	364.39	354.55

Table S3. Sheet resistance of 2 mm and 5 mm pitch at different anilox volumes and printing speeds measured with a multimeter in large area (10 squares).

Sheet Resistance [Ω/sq]			
Pitch, Anilox Volume	0.2 ms^{-1}	0.4 ms^{-1}	0.75 ms^{-1}
5 mm / 5, 1.5 ml m^{-2}	5.187	4.435	4.908
5 mm / 5, 4 ml m^{-2}	2.087	1.777	2.017
5 mm / 5, 10 ml m^{-2}	1.423	1.009	1.033
2 mm / 5, 4 ml m^{-2}	1.067	0.9	0.973

Table S4. Roughness of different samples at different printing speeds.

Roughness [nm]			
Sample	0.2 ms^{-1}	0.4 ms^{-1}	0.75 ms^{-1}
1.5 ml m^{-2} / 5 *mm*	66.60	32.40	73.00
4 ml m^{-2} / 5 *mm*	114.65	82.87	113.36
10 ml m^{-2} / 5 *mm*	39.87	38.69	35.96
4 ml m^{-2} / 2 *mm*	71.90	38.91	43.02

Although this study did not focus on mechanical stability, we note that for the chosen printing parameters mechanical stability was not a signficant concern during the printing and measurement process. Mechanical stability as a function of age would be an interesting topic to investigate. During the course of this work we also numerically investigated shorting through the light harvesting layer which could be caused by a contact with high roughness, we found if the layer was shorted significant electrical losses would occur. Thus contact layers with high roughness should be avoided.

Table S5. Maximum peak and valley for different substrates at different printing speeds.

Peak/Valley [nm]			
Sample	0.2 ms^{-1}	0.4 ms^{-1}	0.75 ms^{-1}
1.5 ml m^{-2}/5 *mm*	439.00/163.97	169.61/106.15	753.08/160.11
4 ml m^{-2}/5 *mm*	542.97/337.66	558.22/342.24	569.75/360.41
10 ml m^{-2}/5 *mm*	373.89/249.92	463.03/364.77	463.03/355.33
4 ml m^{-2}/2 *mm*	483.30/357.22	272.02/378.30	481.15/414.72

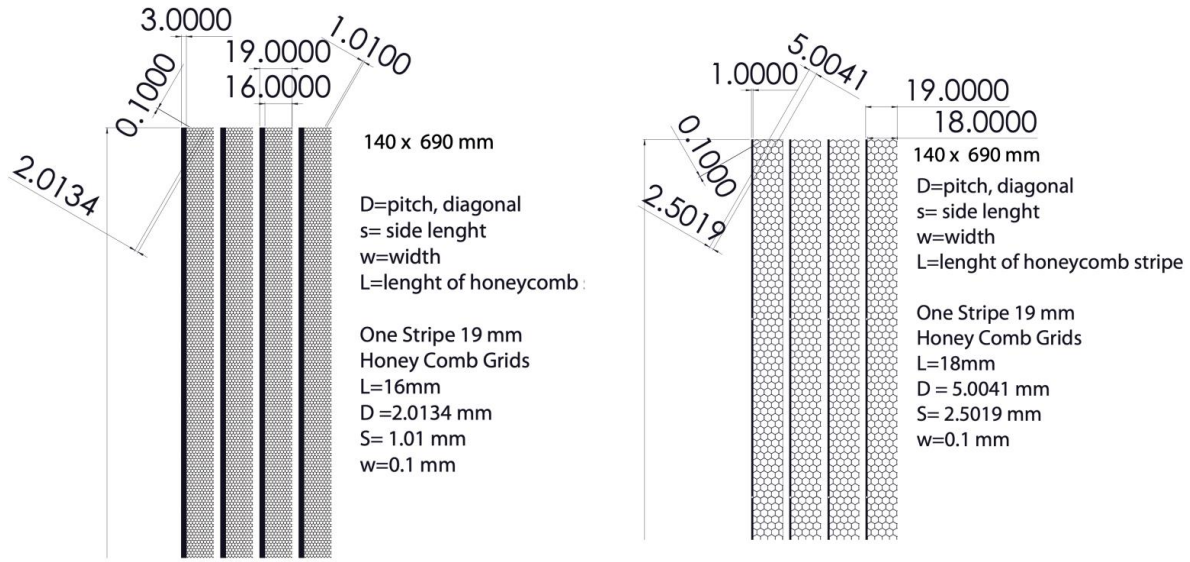

Example structures of printed grids

Figure S1. Example drawings of the printed structures.

Asymmetric grids

Figure S2 plots fill factor, PCE, Voc and Jsc for devices where the honeycomb grid is non symmetric, that is that one side is longer than the other for a fixed line width. It can be seen that it does not matter what the ratio of height to width is, however large structures generally

outperform in terms of PCE smaller structures, although it is worth noting that fill factor for larger cells will drop due to the added series resistance.

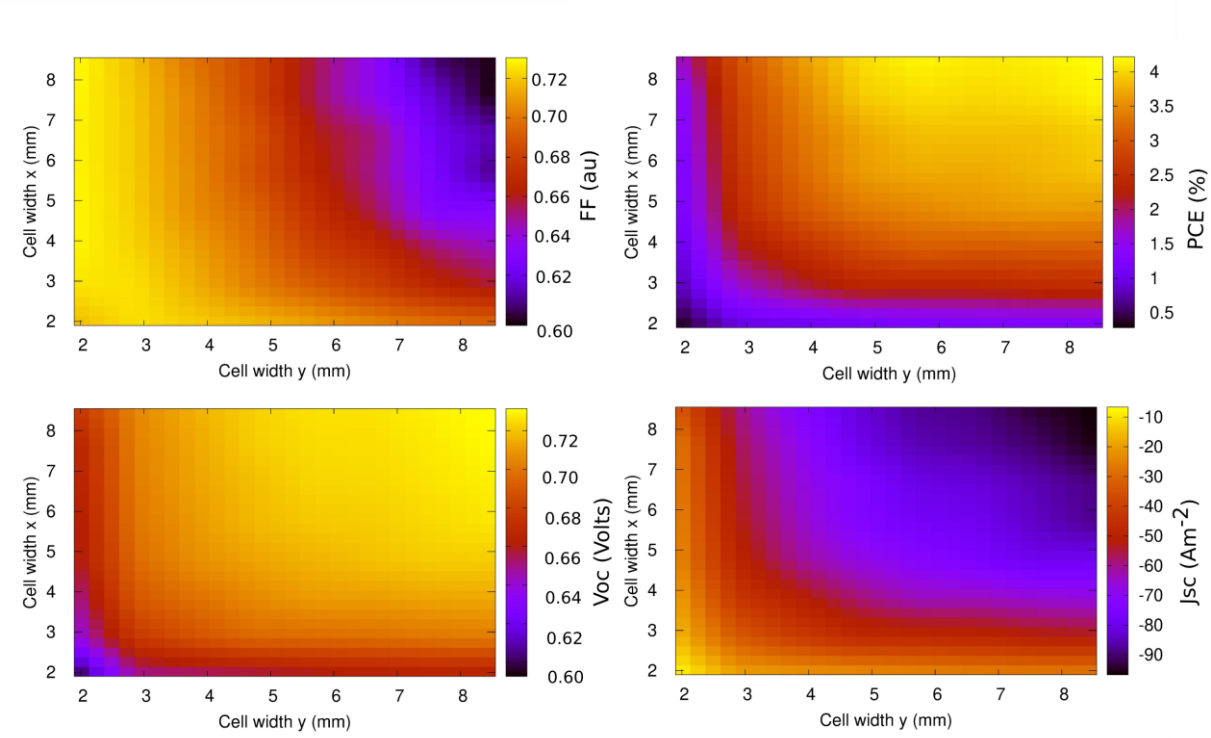

Figure S2. Clock wise, fill factor, PCE, V_{oc} and J_{sc} for the simulated PM6:Y6 structure for asymmetric honeycomb structures, where one side is longer than the other.

Detailed description of the model

The *general purpose photovoltaic device model* (www.gpvdm.com) was extended for this work to be able to solve 3D electrical circuit problems with complex geometries. The changes to the model to allow this are described below.

Construction of the simulation scene: Contacts and device layers are represented by a json object which describes it's location, size and material properties. The json objects are stored in a tree representing the device structure. Linked to each object is a 3D triangular mesh, which forms a closed surface defining the object. Triangular meshes were formed by hand for simple shapes such as boxes, but for more complex shapes such as the honeycomb grids were

formed by discretizing a flat 2D image of the object on the xy plane, the z-height of the mesh were dictated by the intensity of the pixels on the 2D image. Many methods have been proposed to perform this technique,[S1] however we chose to initially mesh the shapes area with a dense uniform triangular mesh, then perform vertex removal to minimize the number of triangles representing the object.[S2] In this way 2D shapes could readily be drawn and turned into 3D shapes. Once all shapes were defined, the scene to be simulated was built in 3D space.

Optical simulation: The space defining the grid was discretize in 3D and the photon distribution within the device calculated using the transfer matrix method[S3,S4] in vertical 1D strips. The equations were solves as a function of wavelength with the AM1.5G spectra used as an input. The total number of photos absorbed within the active layer were integrated over space and assigned to the generation term (I_0) in the closest diode.

Shape identification: Key to performing 3D simulations to be able to link a Cartesian point in space to a 3D object. This was done by projecting a ray vertically from the point of interest and identifying which triangles the ray passed through. If the ray passed through an even number of triangles belonging to an object then the Cartesian coordinate is outside the object, if the ray passed through an odd number of triangles belonging to an object then the Cartesian point is inside that object.

Electrical simulation: To perform electrical simulation the device was again discretized using a finite difference mesh in the xz-plane (that normal to the incident light), mesh points were skipped where no material was present. Vertically under each xz mesh point, a single resistor was used to simulate the resistance of each layer, while four in plane resistors were used to connect the node to the adjoining mesh points (see figure 3c in the main body of the text). The active layer was represented with an equivalent diode circuit.[S5,S6]

Computational acceleration: 3D resistive maps were time consuming to calculate, the solver was therefore threaded with a job handling system to enable efficient load balancing across all CPU cores.

Visualization: Visualization of the results and the electrical mesh were done using OpenGL, object picking was done using false color rendering on an off screen buffer.

[S1] M. Garland and P. S. Heckbert, "Fast polygonal approximation of terrains and height fields", 1995, http://ra.adm.cs.cmu.edu/anon/usr/ftp/usr0/ftp/1995/CMU-CS-95-181.pdf

[S2] W. J. Schroeder, J. A. Zarge, W. E. Lorensen, In *Proceedings of the 19th annual conference on Computer graphics and interactive techniques*. **1992** 65–70.

[S3]T. Zhan, X. Shi, Y. Dai, X. Liu, and J. Zi. Journal of Physics: Condensed, Matter, **2013**, 25 215301.

[S4] P. Peumans, A. Yakimov, and S. R. Forrest. Journal of Applied Physics, **2003**, 93 3693-3723.

[S5] P. O. Grabitz, U. Rau, and J. H. Werner, physica status solidi (a), **2005**, 202, 2920 – 2927

[S6] S. Eidelloth, F. Haase, and R. Brendel, IEEE Journal of Photovoltaics, 2012, 2, 572-578

TOC text

50-60 word summary: Using a combination of gravure/flexographic printing and numerical modelling we evaluate the performance of PEDOT:PSS/Ag hexagonal contact structures for flexible opto-electronic devices. We then take a small area device and numerically estimate how efficient it would be were it upscaled using our printed contacts. This technique allows one to understand how a full device stack would perform before it is deposited, we dub this technique virtual upscaling.

TOC Image